Advanced Steel Construction – Vol. 18 No. 4 (2022) 826–835
DOI:10.18057/IJASC.2022.18.4.10

MECHANICAL PROPERTIES OF HGMFSST COLUMNS UNDER AXIAL COMPRESSION-EXPERIMENT AND ANALYSIS

Yan Zhou, Yu-Tong Duan, Hong-Gang Lei *, Fu-Yu Lu, Xin-Yu Chang and Tie-Ying Li

College of Civil Engineering, Taiyuan University of Technology, Shanxi 030024, China
** (Corresponding author: E-mail: lhgang168@126.com)*

ABSTRACT

High-strength grouting material (HGM) has the characteristics of early strength, high strength, high self-flow, and micro-expansion, but research on composite columns formed by steel tube and HGM is relatively scarce. Therefore, in this paper, the mechanical properties of HGM-filled square steel-tube columns (HGMFSST columns) under axial compression were experimentally studied. The main parameters included tube thickness (t) and HGM strength (fck). The test results showed that members with t = 4 mm failed due to local buckling, and members with thicker steel tube thickness failed mainly due to overall buckling. The measured and predicted ultimate bearing capacity values of the HGMFSST columns based on the existing standards of GB 50936-2014, CECS 159: 2004, AISC/ANSI 360-16, EC4, and AS/NZS 2327: 2017 were compared. The ultimate bearing capacity derived with CECS 159: 2004 was the closest to the measured values and had minimum discreteness.

ARTICLE HISTORY

Received: 14 July 2022
Revised: 14 October 2022
Accepted: 19 October 2022

KEYWORDS

Square steel tube;
High-strength grouting material;
Ultimate capacity;
Strength factor;
Ductility

1. Introduction

High-strength grouting material (HGM) contains well-graded aggregates, cement, and special chemical additives, which enable HGM to achieve high early and final strengths and free-flowing property, and prevent shrinkage upon setting. Currently, a lot of experimental and theoretical studies on the flow performance[1-4] and expansibility[5] of HGM have been carried out. These studies show that the use of HGM can help prevent plastic settlement at the initial stage owing to their free-flowing property and special plastic expansibility. This leads to a high level of compactness and avoids hollowing of infilled material during the pouring process.

As for concrete-filled steel tube (CFST) members, hollowing and voids are generated naturally during the pouring of core concrete due to poor vibration, stiffeners, and reinforcement framework inside the steel tube[6-8]. They affect the bonding ability between the inner concrete and steel tube and reduce the bearing capacity of CFST members[9]. Some studies have shown that increasing the bond performance[10], density[11, 12] and expansibility[13, 14] of core concrete can improve the bonding strength and consequently elevate the bearing capacity of CFST members.

Considering the advantages of HGM, its use as a filling material in square steel tube columns is regarded as a practical structural application. However, current research on HGM-filled square steel-tube (SST) columns (HGMFSST columns) is limited, and the application of HGM mainly focuses on two fields. On the one hand, HGM has been used as a primary medium for load transfer in reinforcement sleeve grouting connection joints, and relevant research mainly focuses on bonding strength and interaction between grout and reinforcement through monotonic tensile[15-17] and cyclic load tests[18, 19]. On the other hand, HGM has been used as a reinforcement material for structures or components. It enables pouring of foundations and supports with large volumes, dense reinforcement, and small spacing with high fluidity[20]. In addition, the use of HGM instead of ordinary concrete in some special projects overcomes the problems of poor compactness and self-shrinking[21, 22]. These two applications indicate that HGM has high fluidity, better bond behavior, and micro-expansion.

Therefore, it is meaningful to study the mechanical properties of composite columns formed by HGM and steel tubes. In this paper, the failure patterns and ultimate bearing capacity of HGMFSST members were studied by axial compression test, and the effect of the tube thickness and HGM strength on the mechanical properties of the members was investigated. The ultimate bearing capacity of the HGMFSST members was predicted and analyzed based on existing standards including GB 50936-2014[23], CECS 159: 2004[24], AISC/ANSI 360-16[25], EC4[26] and AS/NZS 2327: 2017[27].

2. Experimental study

2.1. Specimen preparation

A total of eight members were tested, including six HGMFSST columns and two hollow steel tube (HST) columns as a comparison. Fig. 1 shows schematic views of the HST and HGMFSST columns. The main parameters of the components included tube thickness and HGM strength. The steel tubes selected were Q355-grade high-frequency welded square steel tubes with cross-sectional dimensions of 100 mm × 4 mm and 100 mm × 6 mm. The HGMs used in this test were commercially available finished grouting materials. The strengths of the HGM were determined through material property tests. End plates were welded on both upper and lower ends of the columns. To facilitate the pouring of HGMs, a circular hole with a diameter of 50mm was drilled in the middle of the upper end plate of every column.

The basic parameters of the columns are shown in Table 1. The HGMs used with different strengths were denoted as HGM1, HGM2, and HGM3 respectively. The test members were labelled based on the sectional form of the steel tubes, HGM type, and tube thickness. For example, S-HGM1-4 corresponded to a square steel tube with a thickness of 4 mm, and the in-filled grouting material was HGM1. The members were classified into two groups, namely group I and group II. The length of the members was 1500 mm, approximately half the height of an ordinary residential floor. Table 1 shows the width (B) of the cross-section, the steel tube wall thickness (t), the length (L) and the slenderness ratio (λ) of the members.

Table 1
The basic parameters of the members

No.	Group	Member label	L (mm)	B (mm)	t (mm)	λ	HGM type
1	I	S-4	1500	100	4	26.8	—
2		S-HGM1-4	1500	100	4	23.7	HGM1
3		S-HGM2-4	1500	100	4	24.0	HGM2
4		S-HGM3-4	1500	100	4	24.7	HGM3
5	II	S-6	1500	100	6	27.3	—
6		S-HGM1-6	1500	100	6	25.0	HGM1
7		S-HGM2-6	1500	100	6	25.2	HGM2
8		S-HGM3-6	1500	100	6	26.0	HGM3

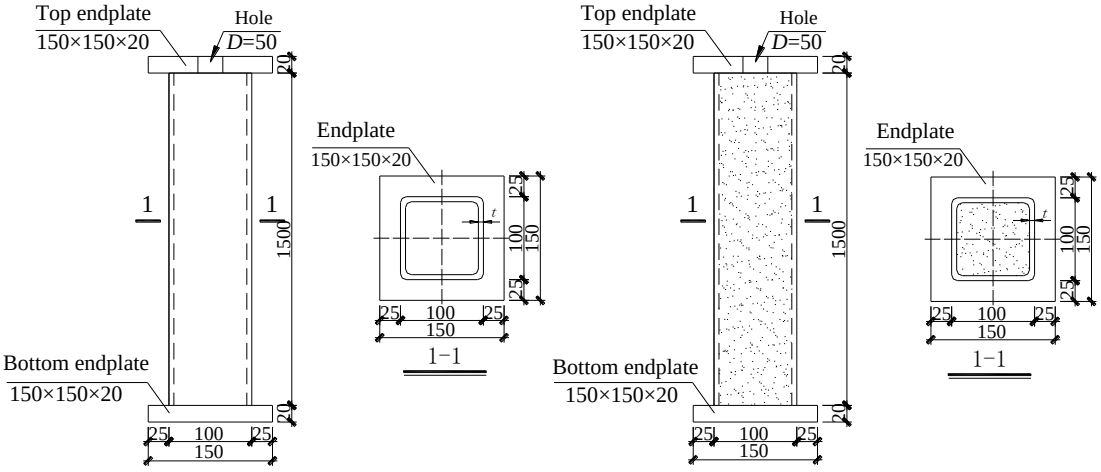

Fig. 1 Schematic views of the HST and HGMFSST members

2.2. Material properties

2.2.1. Steel

The mean values of the mechanical properties of Q355-grade steel are listed in Table 2, including steel plate thickness (t), yield strength (f_y), ultimate strength (f_u), elastic Young's modulus (E_s), percentage elongation (Δ%), and yield strain (f_y/E_s).

Table 2
Material properties of Q355-grade steel

Size	t (mm)	f_y (MPa)	f_u (MPa)	f_y/f_u	E_s (MPa)	Δ (%)	Yield strain ($\mu\varepsilon$)
□100×4	3.72	405.0	621.50	0.652	197991	29.38	2045
□100×6	5.74	467.9	659.70	0.709	195352	24.96	2405

2.2.2. HGM

Based on GB/T 50448-2015[28] and GB/T 50081-2019[29], nine 100 mm × 100 mm × 100 mm cubic blocks were made for each type of HGM to test the cube compression strength (f_{cu}) at Day 3, Day 7, and Day 28. Six 100 mm × 100 mm × 300 mm prismatic blocks were made for each type of HGM to determine the axial compressive strength (f_c) and elastic modulus at Day 28.

Each type of grouting material was prepared by adding a correct amount of water, pouring the mixture into a mixer, and mixing it for 300 s. The mixture was then poured into moulds and released after 24 h. After removal from the moulds, the grouting material members were wrapped with plastic and kept in a maintenance room for 3, 7, and 28 d respectively for the compressive strength experiments. Each specimen was labelled. The members were maintained as shown in Fig. 2.

(1) Cube compressive strength (f_{cu})

Cube compressive strength f_{cu} is not only an essential index for evaluating concrete strength grades, but also a basic index for calculating other mechanical properties. The compressive strengths of the grouting blocks at Day 3, Day 7, and Day 28 were measured using a STYE-2000 pressure testing machine.

The failure modes of HGM1exhibited pyramidal failure forms, which were similar to those of ordinary concrete at Day 3, Day 7, and Day 28. The main phenomenon was the bond failure between aggregate and mortar. No aggregate cracking was found. Unlike HGM1, the failure modes of grouting materials HGM2 and HGM3 originated from vertical cracks, and finally developed into multiple small cylinders. Weak sounds were heard during the loading process. After the strength reached its peak value, loud sounds were produced, which was caused by fracturing of blocks and falling of debris. The typical failure modes of the cube members at Day 3, Day 7, and Day 28 are shown in Fig. 3.

Fig. 2 Maintenance of test blocks

	HGM1	HGM2	HGM3
3-day			

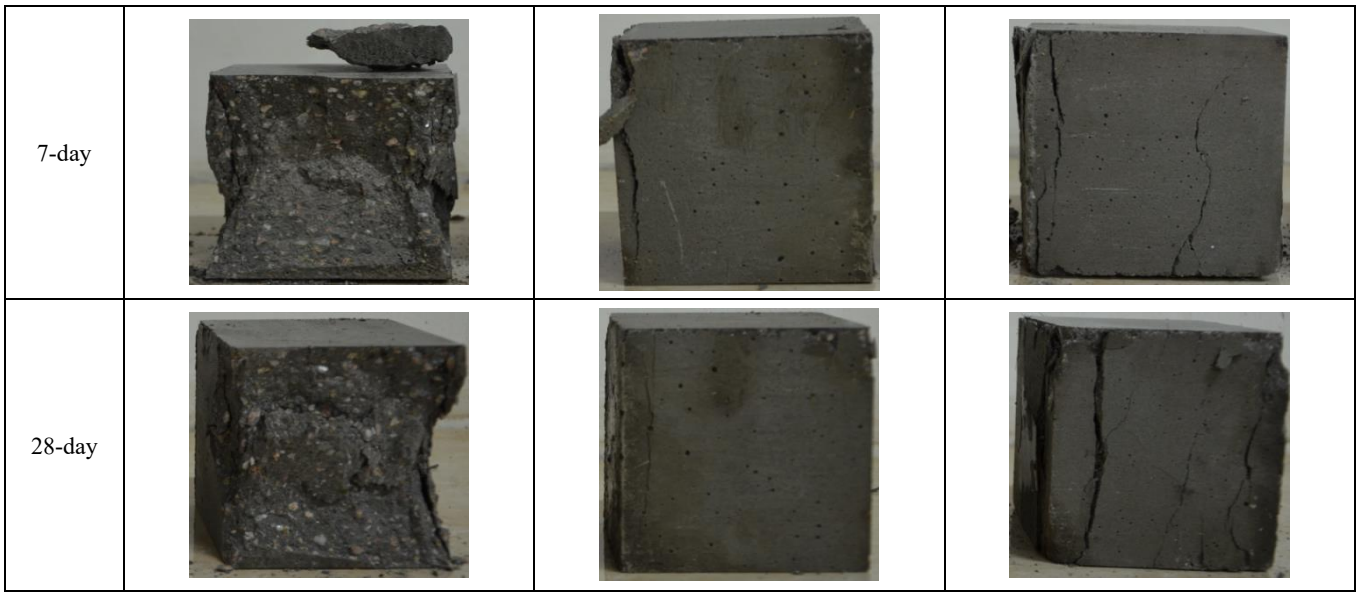

Fig. 3 Failure modes of cube blocks

The mean values of the cube compression strength of the three grouting materials are shown in Table 3. All the blocks had high early strengths, and the strengths increased slowly in later stages.

Table 3
Mechanical properties test results of HGM

HGM type	Cube compression strength f_{cu} (MPa)			Axial compressive strength f_c (MPa)	Elastic moduli E_c (MPa)
	day 3	day 7	day 28		
HGM1	47.6	60.5	74.8	62.3	3.38×10^4
HGM2	51.2	60.2	79.1	67.5	3.47×10^4
HGM3	95.3	107.3	125.6	100.5	4.27×10^4

(2) Axial compressive strength

The friction force between the testing machine and the contact surface of members had a confinement effect on the members in the cube compressive strength test, which affected the actual compression of the materials. Therefore, the axial compressive strength of the prismatic blocks was considered to be a true reflection of the concrete strength, which weakened the confinement effect[30]. The axial compressive strength of the grout prismatic blocks at Day 28 was measured according to the requirements of the standards [28] and [29].

As shown in Fig. 4, the failure states of the prismatic members occurred with the cracks penetrating through the upper and lower bearing surfaces along the diagonal of the blocks. The members in the middle part were dominated by some vertical cracks, because this part of the specimen did not experience the confinement effect of the testing machine and was therefore in a state of uniform compression. The HGM3 test blocks were kept intact with no falling debris, which was due to the presence of steel fibers in this type of grouting material. As can be seen from the crack surface of the HGM3 blocks after test, the steel fibers were pulled out without breaking. HGM1 and HGM2 blocks largely broke into two pieces along the cracks that penetrated the diagonal of the blocks. All the members cracked with loud sounds when the maximum strength was reached. The mean values of the axial compressive strengths of the prismatic members are shown in Table 3.

(3) Elastic modulus

The elastic modulus of a material is the main index of its deformation performance in elastic stage. The elastic moduli of the HGMs were measured according to standard [29], and the mean values are listed in Table 3.

(a) HGM1 (b) HGM2 (c) HGM3

Fig. 4 Failure states of the prismatic members

2.3. Loading device and scheme

The loading device presented in Fig. 5 was operated with a spherical hinge bearing on the top endplate, and the bottom endplate was directly connected to the test bed, where the desired loading conditions were achieved by using a hinged joint on one endplate and a fixed one on the other. Two displacement transducers (D1 and D2) were placed between the two endplates to measure longitudinal displacement, and lateral deformation was measured in the middle section of the members using two displacement transducers (D3 and D4), which were placed perpendicular to each other. Longitudinal and transverse strain gauges were arranged around the columns on the outer surface of a mid-height tube (Section A-A) to measure strain of the members, and four more strain gauges were arranged to measure longitudinal strains at Section B-B.

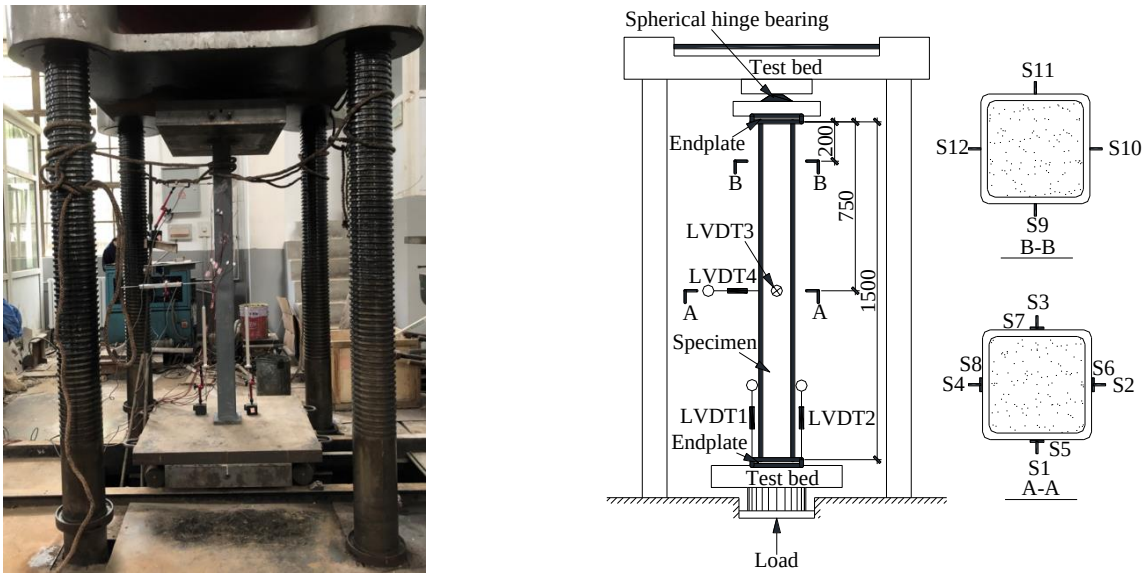

(a) Specimen (b) Instrumentation

Fig. 5 Test setup and instrumentation layout

A multistage loading approach was adopted in the test process. The load control mode was applied until the members reached 75% of the estimated ultimate load. After 75% of the estimated ultimate load was achieved, the displacement was adjusted at a rate of 0.005 mm/s. The tests were stopped when the deformation of the members was too large or the bearing capacity of the members dropped to 80% of the ultimate bearing capacity.

3. Experimental results and discussion

3.1. Failure pattern

Based on the test results, the failure patterns could be classified into two groups: (a) failure with both local buckling and overall buckling (Group I) and (b) failure with only overall buckling (Group II). The observed failure patterns of the tested members are shown in Fig. 6.

During the initial stage of loading, all the members were in an elastic stage. When the load reached approximately 85% of the ultimate bearing capacity, local buckling occurred in the middle of member S-4, upper point of trisection of member S-HGM1-4 relative to the top endplate, and the middle of member S-HGM2-4. As the load was increased, slight bending occurred at the points of local buckling. After reaching the ultimate value, the bearing capacity decreased rapidly with significant bending, and the bulge developed to the adjacent surface. The failure pattern of member S-HGM3-4 was similar to that of the first three members before reaching the ultimate bearing capacity. In the decline stage of the bearing capacity, the bearing capacity underwent a fluctuating decline owing to the presence of steel fibers, which enhanced the ductility of grouting HGM3.

During the whole loading process, due to the thicker steel tube wall, the members of Group II did not have the same local buckling phenomenon as the members of Group I, but the bending phenomenon occurred in the middle of all members. For member S-HGM3-6, when the load decreased to approximately $0.815N_{ue}$, an inflection point occurred in the load-deflection curve owing to the presence of steel fibers, as in the case of member S-HGM3-4. After the load was increased to approximately $0.853N_{ue}$, the bearing capacity gradually decreased, and bending of the member became increasingly obvious.

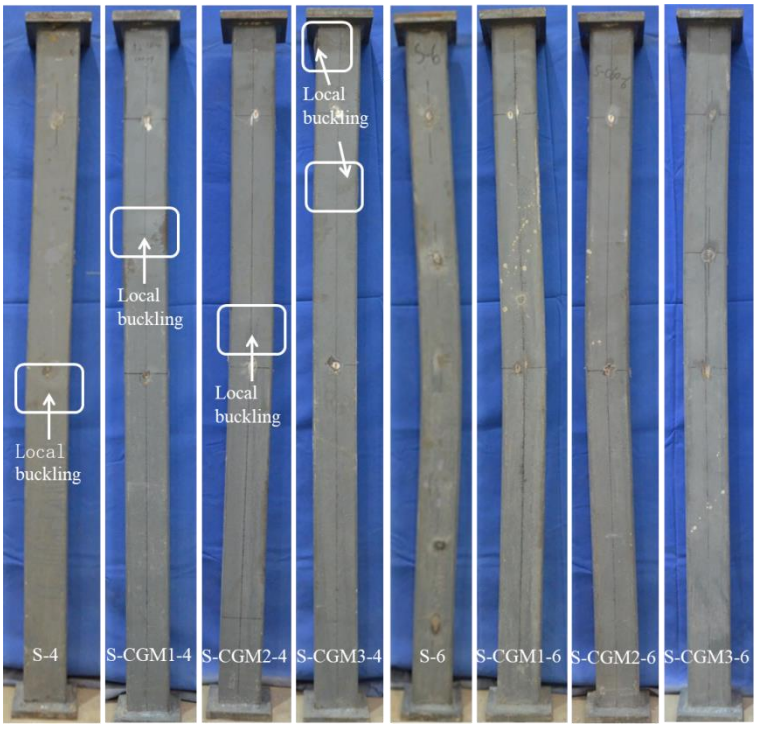

Fig. 6 Failure pattern of tested members

3.2. Load-displacement relationship

3.2.1. Effect of HGM strength

The measured ultimate bearing capacity (N_{ue}) and axial load (N) versus displacement (Δ) relationship are presented in Table 4 and Fig. 7, respectively. The nominal member capacity N_{es} was calculated using the equation $N_{es} = f_y A_s + f_c A_c$, where f_y is the yield strength of steel, f_c is the axial compressive strength of the inner HGM (Table 4), and A_s and A_c are the cross-sectional areas of the tube and the inner HGM, respectively. ξ is the confinement factor ($\xi = A_s f / A_c f_c$), and f is the compressive strength design values of steel. $\Delta_{e85\%}$ is the vertical deformation when the bearing capacity is reduced to 85% of the ultimate bearing capacity, and Δ_{ue} is the vertical deformation corresponding to N_{ue} of a tested member. ω_e is the increase in the ultimate bearing capacity compared with the HST. ω_{es} is the increase in the nominal member capacity compared with the HST. *SI* is the strength index of the member. *DI* is the ductility index of the member.

Table 4
Summary of test results

Group	Specimen label	Ultimate point		$\Delta_{e85\%}$/mm	ω_e (%)	N_{es}/kN	ω_{es}(%)	ω_e/ω_{es}	ξ	*SI*	*DI*
		N_{ue}/kN	Δ_{ue}/mm								
I	S-4	630	6.30	8.18	—	622	—	—	—	1.013	1.334
	S-HGM1-4	1295	5.88	6.33	105.5	1149	84.8	1.245	1.180	1.127	1.076
	S-HGM2-4	1294	5.85	6.30	105.4	1226	97.1	1.085	1.089	1.055	1.077
	S-HGM3-4	1554	5.97	6.40	146.6	1473	136.7	1.072	0.731	1.055	1.072
II	S-6	1013	8.40	26.06	—	1056	—	—	—	0.960	3.102
	S-HGM1-6	1516	7.08	13.76	49.6	1538	45.7	1.085	2.188	0.985	1.943
	S-HGM2-6	1587	6.57	10.13	56.7	1609	52.4	1.082	2.019	0.987	1.542
	S-HGM3-6	1778	6.93	8.61	75.5	1834	73.7	1.023	1.356	0.969	1.241

Table 4 and Fig. 7 show that the ultimate capacity of the members significantly improved after HGM pouring, and the ultimate values improved with an increase in the strength of the HGMs. The ultimate capacities of members S-HGM1-4, S-HGM2-4, and S-HGM3-4 increased by 105.5%, 104.4%, and 146.6%, respectively, compared with the hollow tube specimen S-4. Though the ultimate capacities of members in Group II didn't increase as significantly as those in Group I, they were 49.6%–75.5% higher than that of the hollow tube specimen S-6. This is because the local buckling of the steel tube was effectively suppressed by the inner HGM that had a larger restraint effect on members of Group I. Table 4 shows that ω_e was larger than ω_{es} for HGMFSST members compared with the HST under compression. This illustrates the advantages of combining steel and HGM in HGMFSST composite members: The performance of such combination is greater than the simple sum of HGM and steel tube.

The effect of HGM strength on the load-displacement curves is shown in Fig. 7. As shown in the figure, the whole loading process of the test members could be divided into three stages: elastic stage, elastic-plastic stage, and decline stage. In the initial stage of loading (the elastic stage), the curve slope of the HGMFSST members was significantly larger than that of the steel tube without HGM inside, indicating that the overall initial stiffness of the steel tube members was significantly improved after HGM pouring and increased slowly with the increase of HMG strength. As the applied load was further increased, the growth rate of the vertical displacement gradually accelerated before the ultimate value was reached, and the growth rate of the bearing capacity of the members gradually decreased, which is the elastic-plastic stage.

After the bearing capacity of the members reached the peak load, it began to decrease, but the vertical displacement continued to increase. Consequently, the load-displacement curves of the members entered the decline stage. At the beginning of the decline stage, the descent speed of the bearing capacity of the HGMFSST members was faster than that of the hollow members owing to the abrupt cracking of the HGMs when the bearing capacity reached the ultimate value. When the load dropped to a certain level, the descent speed gradually decreased because the infilled HGMs became more compact after cracking under the loaded state and a confinement effect was provided by the steel tube.

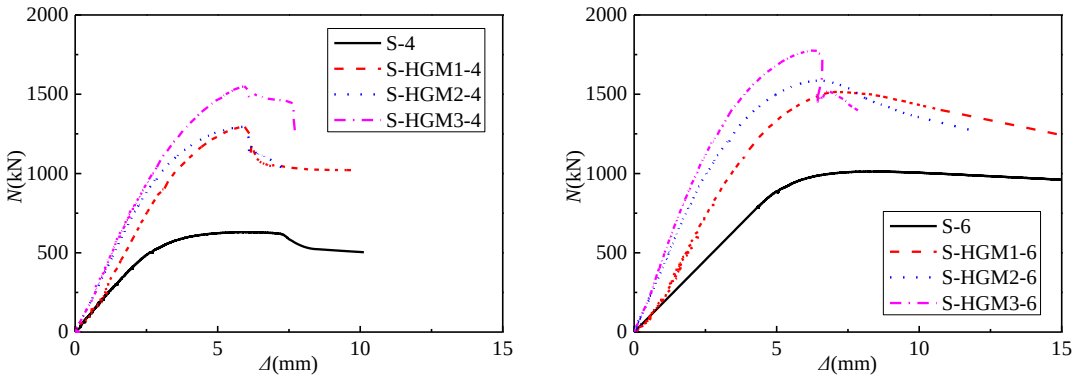

(a) Members of Group I

(b) Members of Group II

Fig. 7 Effect of HGM strength on load-displacement curves

3.2.2. Effect of tube thickness

The load-displacement curves with different tube thicknesses are listed in Fig. 8. As shown in the figure, the curve slopes of the members with different tube thicknesses roughly coincided at the initial loading stage, indicating that the tube thickness had little effect on the overall initial stiffness of the members. Meanwhile, the ultimate bearing capacity of the members increased with the increase of the tube thickness. After the bearing capacity reached the ultimate level, the decrease in the bearing capacity of members of Group II was lower than that of members of Group I. This was because the increase in the tube thickness effectively delayed the local buckling of the steel tube and improved the ductility of the members.

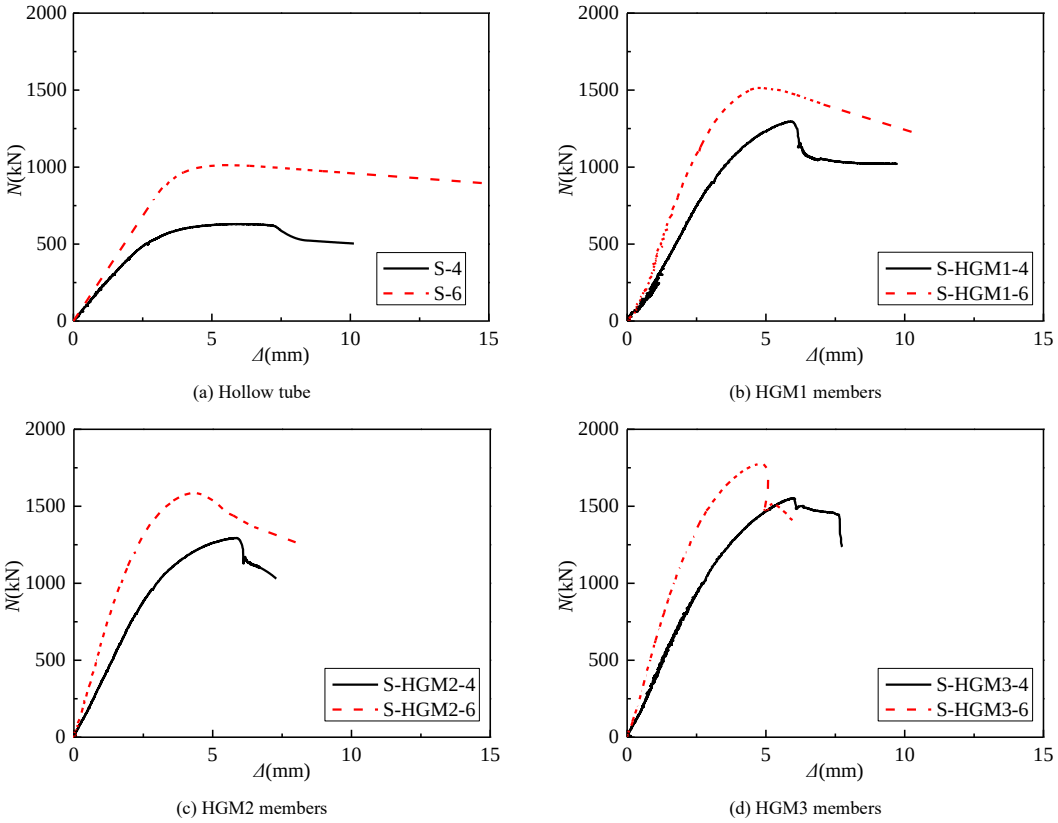

(a) Hollow tube (b) HGM1 members

(c) HGM2 members (d) HGM3 members

Fig. 8 Effect of steel tube thickness on load-displacement curves

3.3. Strength index

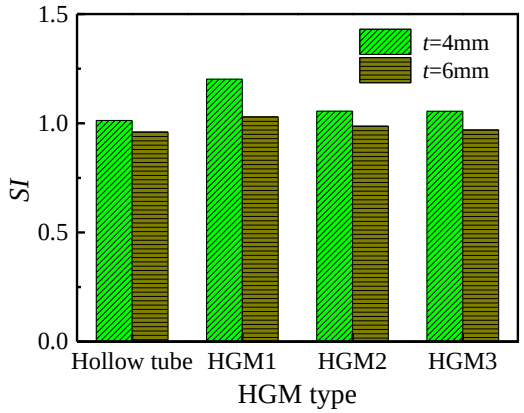

Fig. 9 *SI* of the members

The strength index (*SI*) can be calculated in this study with the following formula defined by Yang[31] and Han[32].

$$SI=\frac{N_{ue}}{N_{es}} \quad (1)$$

Table 4 and Fig. 9 show the strength indices of the members. It can be seen that the *SI* of HST improved after HGM pouring. This was because the inner HGM delayed the local buckling of the steel tube, and the influence was more significant for the thinner steel tube members. In addition, the *SI* of the HGMFSST members slightly decreased with the increase in the HGM strength, which was mainly because the increase in the HGM strength reduced the constraint effect (Table 4) of the steel tube on the inner HGM[32].

3.4. Ductility index

The ductility index (*DI*) can be calculated using the following formula defined by Ge [33] and Zhao[34]:

$$DI=\frac{\Delta_{e85\%}}{\Delta_{ue}} \quad (2)$$

Table 4 and Fig. 10 show the ductility indices of the members. The *DI* of the HGMFSST members decreased with an increase in the HGM strength. This can be explained with the confinement factor ξ, because the constraint effect of the steel tube on the inner HGM decreased with an increase in the HGM strength. Compared with the HGMFSST members of Group II, the effect of the HGM strength on the *DI* was minimal for the HGMFSST members of Group I. This was due to the local buckling that occurred easily in members with thinner plates and limited the development of the plastic section. Table 4 shows that the *DI* increased by 80.58%, 43.18%, and 15.76% as the tube thickness was increased for the HGM1, HGM2, and HGM3 members, respectively. In addition, the increase ranges became narrower, indicating that the *DI* gradually became dominated by the infilled HGM with an increase in the HGM strength for the HGMFSST members.

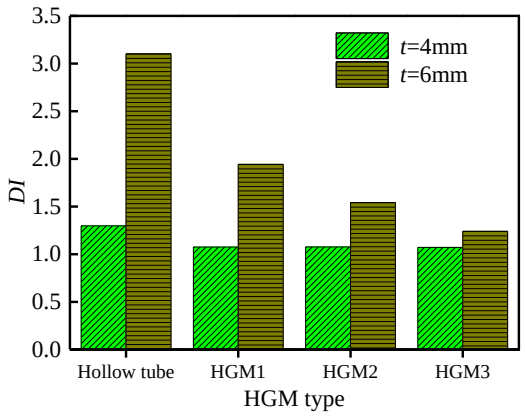

Fig. 10 *DI* of the members

3.5. Load-strain relationships

In order to study the cross-sectional stress distribution of the compressed members, strain gauges were set around the members, and the specific layout is shown in Fig. 5. The strain gauges S1~S4 were used to measure the longitudinal strain of the members and analyze the yielding condition of the steel tube under axial load. The strain gauges S5~S8 were used to measure the transverse strain of the members and analyze the restraint of the steel tube on the inner HGM.

The load-strain relationships are shown in Fig. 11, where ε_y ($\varepsilon_y = f_y/E_s$) is the yield strain of the steel tube, and the positive and negative values represent tensile and compressive strains, respectively. As shown in the figure, prior to reaching the yield strain of the steel, the longitudinal and transverse strains of the members showed a linear upward trend with the increase in the load, and the strains of the four surfaces of the steel tube were almost coincident, indicating that the members were well centered and generally in the state of axial compression. The strain information collected by the strain gauges at the locations of local buckling or bulge can directly reflect the deformation of the members. When the axial load decreased, the longitudinal strain of the tensile surface of the bending part of the steel tube gradually decreased with an increase in the bending deformation, and even lead to tensile strain. Meanwhile, the longitudinal strain of the compressive surface continued to increase. In steel tube parts other than the bending or bulging part, the strain increased gradually with a decrease in the axial compressive load. Taking specimen S-HGM2-6 as an example, strain gauge S2 was on the tension surface at the buckling position, where the measured strain initially increased and then decreased in the loading process. Strain gauge S4 was on the compressive surface of at the buckling position, where the measured strain increased or remained unchanged during the loading.

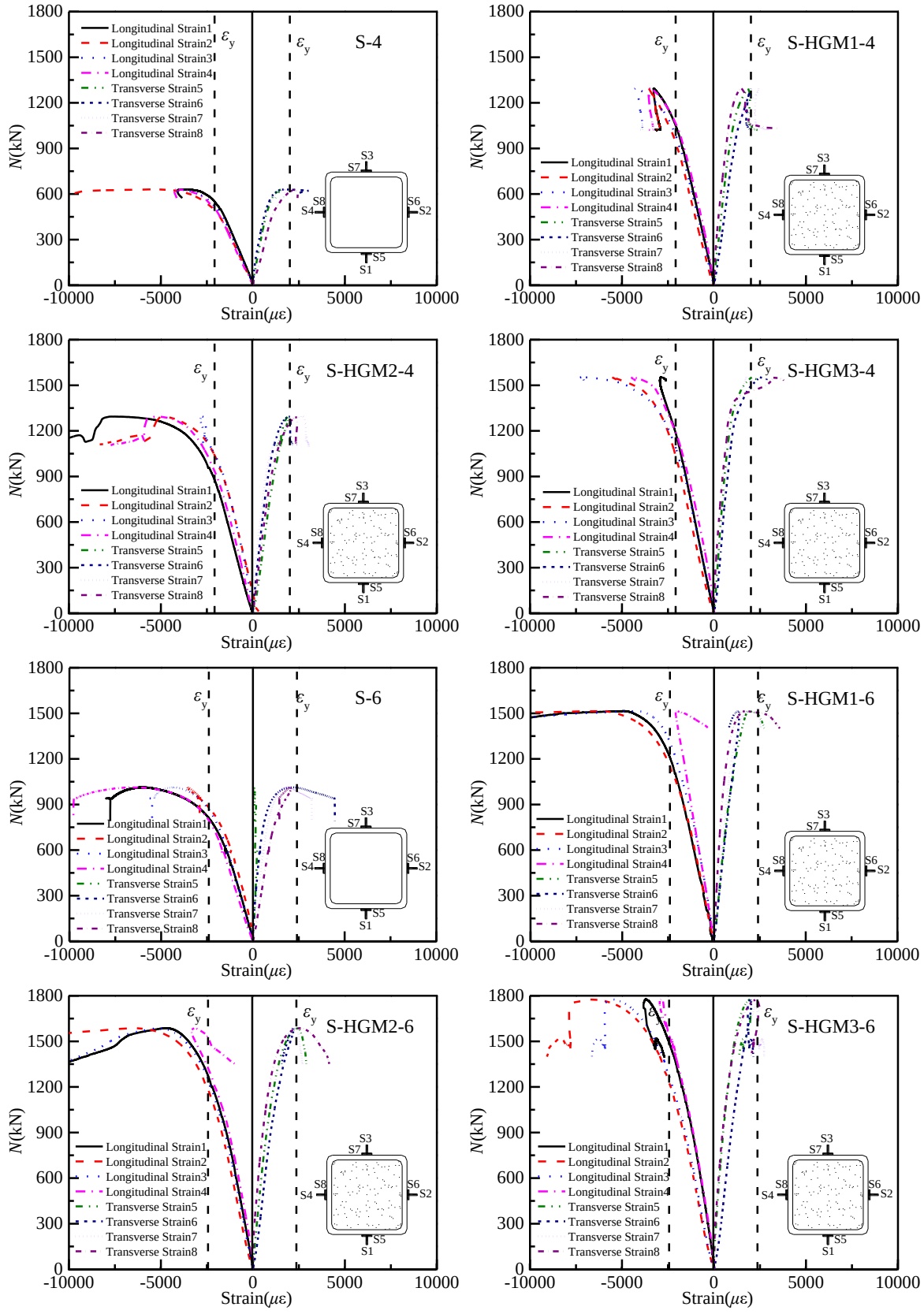

Fig. 11 Load-tube strain responses

The average cross-sectional longitudinal strains in the middle of the members are shown in Fig. 12, where ε_u ($\varepsilon_u = f_u/E_s$) is the ultimate strain of the steel tube.

Fig. 12 shows that the strains of the HGMFSST columns were larger than those of the HSTs at the ultimate load, which is consistent with the experimental finding of Han[35]. In addition, the loading-stain curve slopes of the HGMFSST columns were significantly larger than those of the HST, indicating that the steel tube and inner HGM worked well in conjunction under axial compression. Besides, the increase in the HGM strength had little effect on the longitudinal strains of the HGMFSST members with similar tube thicknesses.

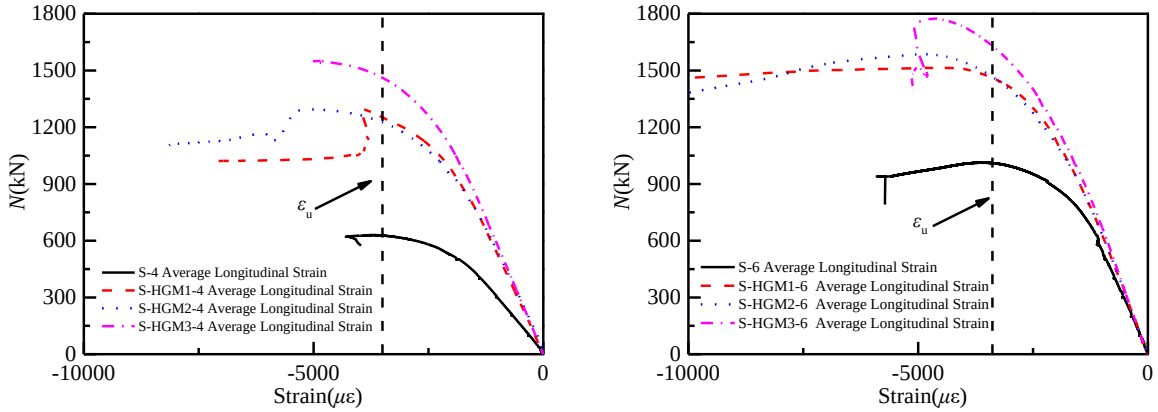

(a) Members with t = 4 mm (b) Members with t = 6 mm

Fig. 12 Average load-tube cross-sectional strain responses in the middle part

4. Prediction of ultimate bearing capacity

The ultimate bearing capacity of structural members is an important indicator of their static performance. Hence, a reliable method for calculating their ultimate strength is essential for practical application of these structural members in engineering design. At present, there is still no common standard for ultimate bearing capacity of HGMFSST members, but Wu[36] pointed out that the constitutive relation of ordinary concrete can be used for HGM after experimental investigation. Therefore, some calculation formulas of ultimate bearing capacity of CFST members were selected in this study to calculate the bearing capacity of the tested HGMFSST members under axial compression. The applicability of these formulas was verified by comparison with the experimental results. The calculation formulas used were derived based on the following standards: GB 50936-2014, CECS 159: 2004, AISC/ANSI 360-16, EC4 and AS/NZS 2327: 2007.

4.1. Calculation formulae

Table 5 lists the calculation formulas for the bearing capacity of CFST members under axial compression based on five standards.

Table 5
Calculation formulae for bearing capacity of CFST members

Standard	Calculation formulae	Formula description
GB 50936-2014	$N = \varphi N_0$; $N_0 = A_{sc} f_{sc}$; $f_{sc} = (1.212 + B\xi + C\xi^2) f_c$; $\xi = A_s f / A_c f_c$	N denotes the design value of stable bearing capacity. N_0 denotes the design value of axial compression strength of a short column. φ denotes the stability factor. A_{sc} denotes the cross-sectional area of a CFST member, $A_{sc} = A_s + A_c$. A_s, and A_c denote the cross-sectional areas of steel tube and inner concrete, respectively. f_{sc} denotes the compressive strength design value of CFST. ξ denotes constraint effect coefficient. f and f_c are the compressive strength design values of steel and concrete, respectively. B and C denote the influence coefficients of the constraint effect.
CECS 159: 2004	$N = \varphi N_0$; $N_0 = f A_s + f_c A_c$ when $\frac{P_{n0}}{P_e} \le 2.25$,	The meaning of each symbol is consistent with that in GB 50936-2014.
AISC/ANSI 360-16	$P_n = P_{n0}\left(0.658^{\frac{P_{n0}}{P_e}}\right)$; when $\frac{P_{n0}}{P_e} > 2.25$, $P_n = 0.877 P_e$; $P_{n0} = f_y A_s + 0.85 f_c' A_c$; $P_e = \pi^2 (EI_{eff})/(KL)^2$	P_n denotes nominal compressive strength. P_{n0} denotes nominal compressive strength of a zero length, doubly symmetric, and axially loaded composite member. P_e denotes elastic critical buckling load. f_y denotes yield stress of steel. f_c' denotes specified compressive strength of concrete. EI_{eff} denotes effective stiffness of a composite section. K denotes effective length factor. L denotes the length of a member.
EC4	$\frac{N_{Ed}}{\chi N_{pl,Rd}} \le 1.0$; $N_{pl,Rd} = A_s f_y + A_c f_c'$	N_{Ed} denotes the design value of compressive normal force. $N_{pl,Rd}$ denotes the design value of the plastic resistance of a composite section to compressive normal force. χ denotes the reduction factor for flexural buckling.
AS/NZS 2327: 2017	$N_{c,Rd} = \alpha_c N_{s,Rd} \le N_{s,Rd}$; $N_{s,Rd} = \emptyset A_s f_y + \emptyset_c A_c f_c'$	$N_{c,Rd}$ denotes member resistance. $N_{s,Rd}$ denotes section resistance. α_c denotes compression member slenderness reduction factor. $\emptyset$ and $\emptyset_c$ denote capacity factor for steel and concrete, respectively, where $\emptyset = 0.9, \emptyset_c = 0.6$.

4.2. Analysis of calculation results

The ultimate bearing capacity (N_u) calculated based on different standards were compared with the test results (N_{ue}) presented in Table 6 and Fig. 13. It can be seen from the table that the five standards used were conservative. The difference between the predicted strengths of the HGMFSST members using GB 50936-2014 and the measured values were in the range of -0.4%–26%. The predicted strengths were lower than the measured values, except for that of member S-HGM3-4 (Table 6). The average ratio and standard deviation of N_u/N_e were 0.892 and 0.074, respectively. Using AISC/ANSI 360-16 and EC4, the member capacity was approximately 12%-25% lower than the measured ultimate strength, and the average N_u/N_e ratios were 1.017 and 0.968 with standard deviations of 0.048 and 0.042, respectively. The predicted strengths obtained using AS/NZS 2327:2017 were approximately 18%-32% lower than the measured values, and the average and standard deviation of N_u/N_e were 0.756 and 0.05, respectively. The predicted strengths obtained using CECS 159:2004 were approximately 2%-15% lower than the measured values, and the average and standard deviation of N_u/N_e were 0.931 and 0.043, respectively. As can be seen, in general, the predicted strengths of the HGMFSST members using the AS/NZS2327: 2017 standard had a minimum average of 0.756, which indicates that this standard was more conservative than the others. The combined analysis of Fig. 13 shows that the predicted values of CECS 159:2004 were closest to the measured values with minimum discreteness for a wide range of design parameter values.

Table 6
Summary table of calculation results

Specimen label	N_{ue}	GB50936-2014		AISC/ANSI 360-16		EC4		AS/NZS2327: 2017		CECS159: 2004	
		$N_{u,GB}$	$N_{u,GB}/N_{ue}$	$N_{u,AISC}$	$N_{u,AISC}/N_{ue}$	$N_{u,EC4}$	$N_{u,EC4}/N_{ue}$	$N_{u,AS}$	$N_{u,AS}/N_{ue}$	$N_{u,CECS}$	$N_{u,CECS}/N_{ue}$
S-HGM1-4	1295	1143	0.882	969	0.748	1045	0.807	888	0.685	1106	0.854
S-HGM2-4	1294	1242	0.959	993	0.767	1080	0.835	911	0.704	1181	0.912
S-HGM3-4	1554	1560	1.004	1253	0.806	1404	0.904	1153	0.742	1417	0.912
S-HGM1-6	1516	1204	0.794	1307	0.862	1337	0.882	1217	0.803	1459	0.963
S-HGM2-6	1587	1295	0.816	1328	0.837	1370	0.863	1240	0.781	1527	0.962
S-HGM3-6	1778	1597	0.898	1564	0.880	1657	0.932	1460	0.821	1743	0.980
Average			0.892		0.817		0.870		0.756		0.931
Standard deviation			0.074		0.048		0.042		0.050		0.043

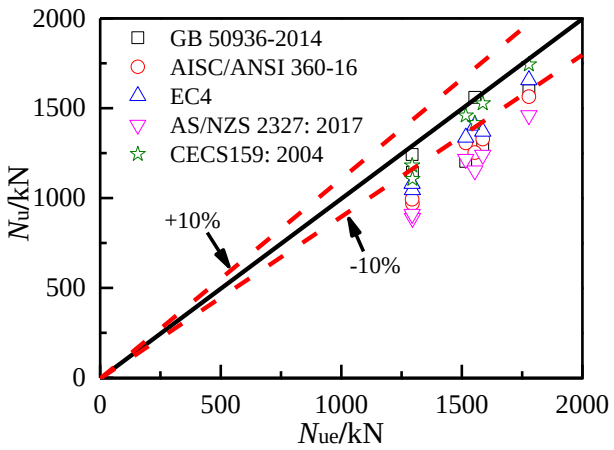

Fig. 13 Comparison of calculation results.

5. Conclusions

The following conclusions can be drawn from the axial compression test and correlation analysis:

(1) Testing of the cube blocks at different ages shows that the failure modes of the grouting materials HGM2 and HGM3 originated from vertical cracks and then developed into multiple small cylinders. These failure modes are different from those of ordinary concrete. In prismatic blocks, the failure modes occurred with the cracks penetrating through the upper and lower bearing surfaces along the diagonal of the blocks. In HGM3, the blocks remained undecomposed after fracture owing to the presence of steel fibers.

(2) The test results show that the members of Group I (t = 4 mm) failed due to both local buckling and overall buckling, whereas the members of Group II (t = 6 mm) failed due to overall buckling.

(3) For the HGMFSST members, the strength and ductility indices decreased with an increase in HGM strength. For the HST members, the strength index improved after HGM pouring because the inner HGM effectively delayed the local buckling of the steel tube.

(4) The load-strain relationships show that the inner HGM effectively delayed the local buckling of the steel tube, and the steel tube and inner HGM worked well in conjunction under axial compression. The HGM can be used as the inner filling material of the steel tube to form a composite member.

(5) Theoretical ultimate strengths of the HGMFSST members were calculated based on existing standards, which were conservative but acceptable. The results predicted with CECS 159: 2004 were the closest to the measured values, with minimum discreteness for a wide range of design parameter values.

Acknowledgements

This study was supported by Enterprise-commissioned Projects (No. HX2021-01).

References

[1] Mirza J, Mirza M S, Roy V, et al. Basic rheological and mechanical properties of high-volume fly ash grouts[J]. Construction & building materials. 2002, 16(6): 353-363.
[2] _ahmaran M, özkan N, Keskin S B, et al. Evaluation of natural zeolite as a viscosity-modifying agent for cement-based grouts[J]. Cement and Concrete Research. 2008, 38(7): 930-937.
[3] Sha F, Li S, Liu R, et al. Experimental study on performance of cement-based grouts admixed with fly ash, bentonite, superplasticizer and water glass[J]. Construction and Building Materials. 2018, 161: 282-291.
[4] Mohammed A, Mahmood W, Ghafor K. Shear stress limit, rheological properties and compressive strength of cement-based grout modified with polymers[J]. Journal of Building Pathology and Rehabilitation. 2020, 5(1).
[5] Zheng-Ming S, Jian-Qi Z, Chao-Ming Z, et al. Properties research on CGM high performance cement-based grout[J]. CONCRETE. 2007(11): 98-101. (in Chinese)
[6] Liao F, Han L, He S. Behavior of CFST short column and beam with initial concrete imperfection: Experiments[J]. Journal of Constructional Steel Research. 2011, 67(12): 1922-1935.
[7] Liao F, Han L, Tao Z. Behaviour of CFST stub columns with initial concrete imperfection: Analysis and calculations[J]. Thin-Walled Structures. 2013, 70: 57-69.
[8] Han L, Ye Y, Liao F. Effects of Core Concrete Initial Imperfection on Performance of Eccentrically Loaded CFST Columns[J]. Journal of Structural Engineering. 2016, 142(12): 1-13.
[9] Liao F Y, Li Y J. Experimental Behaviour of Concrete Filled Steel Tubes (CFST) with Initial Concrete Imperfection Subjected to Eccentric Compression[J]. Applied Mechanics and Materials. 2012, 174-177: 35-38.
[10] Guler S, Lale E, Aydogan M. BEHAVIOUR OF SFRC FILLED STEEL TUBE COLUMNS UNDER AXIAL LOAD[J]. ADVANCED STEEL CONSTRUCTION. 2013, 9(1): 14-25.
[11] Han L. The Influence of Concrete Compaction on the Strength of Concrete Filled Steel Tubes[J]. Advances in structural engineering. 2000, 3(2): 131-137.
[12] Han L, Yao G. Influence of concrete compaction on the strength of concrete-filled steel RHS columns[J]. Journal of Constructional Steel Research. 2003, 59(6): 751-767.
[13] Tao Z, Song T, Uy B, et al. Bond behavior in concrete-filled steel tubes[J]. Journal of Constructional Steel Research. 2016, 120: 81-93.
[14] Yu F, Yao C, Hu Y, et al. AXIAL COMPRESSIVE BEHAVIOR OF SELF-STRESSING STEEL SLAG AGGREGATE CONCRETE FILLED STEEL TUBULAR COLUMNS

WITH BOND-SLIP DAMAGE[J]. Advanced Steel Construction. 2020, 16(1): 13-19.
[15] Einea A, Yamane T, Tadros M K. Grout-Filled Pipe Splices for Precast Concrete Construction[J]. PCI Journal. 1995, 40(1): 82-93.
[16] Ling J H, Abd. Rahman A B, Ibrahim I S. Feasibility study of grouted splice connector under tensile load[J]. Construction and Building Materials. 2014, 50(1): 530-539.
[17] Ling J H, Abd. Rahman A B, Ibrahim I S, et al. Tensile capacity of grouted splice sleeves[J]. Engineering Structures. 2016, 111: 285-296.
[18] Hayashi Y, Nakatsuka T, Miwake I, et al. MECHANICAL PERFORMANCE OF GROUT-FILLED COUPLING STEELSLEEVES UNDER CYCLIC LOADS[J]. Journal of Structural & Construction Engineering. 1997, 496(496): 91-98.
[19] Lin F, Wu X. Mechanical Performance and Stress–Strain Relationships for Grouted Splices Under Tensile and Cyclic Loadings[J]. International Journal of Concrete Structures and Materials. 2016, 10(4): 435-450.
[20] Qun Z, Xiao-Lin Z, Chao-Ming Z. CGM grouting material in gymnasium engineering of Beijing Institute of Technology[J]. Concrete. 2004, 179(9): 66-67, 80. (in Chinese)
[21] Yong-Xin Z, Mu-Xing S, Shu-Nan L, et al. The Application of High-strength Non-shrinkage Grouting Material of the Tail Pipe Steel Lining Replacement[J]. Northeast Electric Power Technology. 2015, 36(5): 8-10. (in Chinese)
[22] Du K. Construction of Two Times Concrete Pouring with High - strength Non - shrinkage Grouting instead of Steel Column Bottom[J]. Architectural Engineering Technology And Design. 2017(19): 1755-1756. (in Chinese)
[23] GB50936-2014, Technical Code for Concrete Filled Steel Tubular Structures[S]. Beijing, 2014.
[24] CECS 159: 2004, Technical specification for structures with Concrete-filled rectangular steel tube members[S]. Beijing, 2004.
[25] ANSI/AISC 360—16. Specification for Structural Steel Buildings[S]. Chicago, 2016.
[26] Eurocode 4. Design of composite steel and concrete structures - Part 1.1: General rules and rules for buildings[S]. Brussels, 2004.
[27] AS/NZS 2327: 2017. Composite structures—Composite steel-concrete construction in buildings[S]. AS/NZE, 2017.
[28] GB/T 50448-2015, Technical code for application of cementitious gout[S]. Beijing, 2015.
[29] GB/T50081-2019, Standard for test Methods of concrete physical and mechanical properties[S]. Beijing, 2019.
[30] Han L H. Concrete Filled Tubular Structures-theory and Practice[M]. Beijing: Science Press, 2004. (in Chinese)
[31] Yang Y, Han L. Compressive and flexural behaviour of recycled aggregate concrete filled steel tubes (RACFST) under short-term loadings[J]. Steel and Composite Structures. 2006, 6(3): 257-284.
[32] Han L H. Tests on stub columns of concrete-filled RHS sections[J]. Journal of Constructional Steel Research. 2002, 58(3): 353-372.
[33] Ge H, Usami T. Cyclic Tests of Concrete-Filled Steel Box Columns[J]. Journal of Structural Engineering. 1996, 122(10): 1169-1177.
[34] Zhao X, Hancock G. Tests to Determine Plate Slenderness Limits for Cold-Formed Rectangular Hollow Sections of Grade C450[J]. Steel Construction. 1991, 25(4).
[35] Han L. Tests on Concrete Filled Steel Tubular Columns with High Slenderness Ratio[J]. Advances in structural engineering. 2000, 3(4): 337-345.
[36] Wu Y, Yang X, Wang K, et al. Experimental study on the stress-strain curve of cementitious grout under uniaxial compression[J]. Industrial Construction. 2014, 151(s1): 909-913, 903. (in Chinese)